Correlation of Rolling Condition, Microstructure, and Low-Temperature Toughness of X70 Pipeline Steels

BYOUNGCHUL HWANG, SUNGHAK LEE, YOUNG MIN KIM, NACK J. KIM, and JANG YONG YOO

Correlation of rolling conditions, microstructure, and low-temperature toughness of high-toughness X70 pipeline steels was investigated in this study. Twelve kinds of steel specimens were fabricated by vacuum-induction melting and hot rolling, and their microstructures were varied by rolling conditions. Charpy V-notch (CVN) impact test and drop-weight tear test (DWTT) were conducted on the rolled steel specimens in order to analyze low-temperature fracture properties. Charpy impact test results indicated that the energy transition temperature (ETT) was below −100 °C when the finish cooling temperature range was 350 °C to 500 °C, showing excellent low-temperature toughness. The ETT increased because of the formation of bainitic ferrite and martensite at low finish cooling temperatures and because of the increase in effective grain size due to the formation of coarse ferrites at high finish cooling temperatures. Most of the specimens also showed excellent DWTT properties as the percent shear area well exceeded 85 pct, irrespective of finish rolling temperatures or finish cooling temperatures, although a large amount of inverse fracture occurred at some finish cooling temperatures.

I. INTRODUCTION

PIPELINE steels used for the transportation of crude oil or natural gas over a long distance under a high pressure primarily require high strength and toughness, and their thickness and diameter tend to increase for lowering transportation cost.[1–7] As natural resources are seriously depleted by industrialization, active oil drilling in extremely cold areas such as Siberia and Alaska is underway. Thus, pipeline steels with excellent low-temperature toughness help transport natural resources at low temperatures for transportation efficiency.

Among currently available methods to evaluate low-temperature toughness of pipeline steels, Charpy V-notch impact test (CVN) and drop-weight tear test (DWTT) are widely used.[8–15] The DWTT was adopted by the American Petroleum Institute (API) in 1965 as the official testing condition for supplying pipeline steels, because it is well consistent with the fracture appearance transition occurring in actual fracture behavior of pipeline steels, its specimens are relatively easy to prepare, and the testing is economical.[11] The 85 pct shear area (pct SA) measured from the DWTT is generally known as the "Battelle 85 pct SA criterion"[7] for the prevention of brittle fracture propagation. Absorption energy measured from the Charpy impact test is used as the value showing the resistance to unstable ductile fracture propagation according to the semiempirical approach of the "Battelle two-curve method" developed by Maxey.[7,9] The absorption energy previously showed certain correlation with resistance to ductile fracture propagation in conventional low-toughness steels. In recently developed high-toughness steels, however, this correlation is less obvious. According to Wilkowski *et al*.,[10] when the absorption energy of Chevron notch DWTT (CN DWTT), which is a modified test method over the conventional pressed notch DWTT (PN DWTT), is used for high-toughness pipeline steels, it provides better average values representing the resistance to ductile fracture propagation, as the fracture path of DWTT specimen is longer than that of Charpy impact specimen. Presently, according to the API 5L3 specification,[11] it is recommended as a requirement for fracture propagation transition temperature (FPTT) of pipeline steels to use CN DWTT specimens for high-toughness steels and PN DWTT specimens for low-toughness steels. The absorption energies of the Charpy impact test, PN DWTT, and CN DWTT all can be used as the criteria to evaluate the resistance against unstable ductile fracture.

In the present study, high-toughness X70 pipeline steel specimens having various microstructures were fabricated by varying rolling conditions, and PN DWTT and CN DWTT, together with Charpy impact test, were conducted on them in order to investigate the effects of microstructure on fracture properties. In addition, effective grain size of these various specimens was investigated using electron backscatter diffraction (EBSD) analysis, and the results were interpreted in relation to low-temperature toughness.

II. EXPERIMENTAL

The steel used in this study was an X70 grade pipeline steel having a yield strength level of over 483 MPa (70 ksi) at room temperature, and its chemical composition is provided in Table I. Twelve kinds of X70 steel specimens were fabricated by varying rolling conditions, as shown in Table II. An overall grain refinement effect was expected by rolling under the rolling reduction ratio of 75 pct in the nonrecrystallized region of austenite after austenitization at 1200 °C. Rolling was started at two temperatures, 980 °C and 910 °C, and finished at two temperatures, 830 °C to 860 °C and 720 °C to 750 °C, which were the temperature in the austenite single-phase region over

BYOUNGCHUL HWANG and YOUNG MIN KIM, Postdoctoral Research Associates, are with the Center for Advanced Aerospace Materials, Pohang University of Science and Technology, Pohang, 790-784, Korea. SUNGHAK LEE and NACK J. KIM, Professors, Center for Advanced Aerospace Materials, Pohang University of Science and Technology, are jointly appointed with Materials Science and Engineering, Pohang University of Science and Technology. Contact e-mail: shlee@postech.ac.kr JANG YONG YOO, Principal Researcher, is with the Plate Research Group, Technical Research Laboratories, POSCO, Pohang 790-785, Korea.

Manuscript submitted October 16, 2003.

Ar_3 and the temperature in the (austenite + ferrite) two-phase region below Ar_3, respectively. After finish rolling, the specimens rolled in the single-phase region began cooling at 780 °C to 810 °C, while the specimens rolled in the two-phase region began cooling at 690 °C to 710 °C. Finish cooling temperature (FCT) was varied in the range from 100 °C to 600 °C, and the cooling rate was about 10 °C/s. The initial and final thicknesses of the steel plates were 150 and 19.1 mm, respectively. Thus, the total rolling reduction ratio was 87 pct. For convenience, the specimens that were rolled in the single-phase region and cooled at different finish cooling temperatures are referred to as "A1" to "A6" specimens, while those rolled in the two-phase region and cooled at different finish cooling temperatures are referred to as "A7" to "A12" specimens.

Specimens were etched using a nital solution for examination by optical microscopy. In addition, secondary phases such as martensite-austenite constituent (MA) and retained austenite (RA) were identified using a two-step etching method,[16] and their volume fraction was measured by an image analyzer. In this two-step etching, specimens were etched first in a solution of 96 pct ethanol, 4 pct picric acid, and a few drops of hydrochloric acid, and were then etched in a solution of sodium hydroxide and metabisulfate. After the two-step etching, ferrite, MA, and RA are shown to be white-colored, brown-colored, and light-blue-colored, respectively. Tensile bars with a gage diameter of 6 mm and a gage length of 30 mm were prepared in the transverse direction, and were tested at room temperature at a crosshead speed of 5 mm/min using a 10-ton Instron (model Instron 8801, Instron Corp., Canton, MA) machine. Charpy impact tests[14] were performed on subsize Charpy V-notch bars with a 7.5 × 10 × 55 mm size, which were machined in the transverse-longitudinal (T-L) orientation, in the temperature range from −196 °C to 20 °C using a impact tester (model FAHC-J-500-1, JT Toshi, Japan) of 500 J capacity. In order to reduce errors in data interpretation, regression analysis for absorbed impact energy *vs* test temperature was done using a hyperbolic tangent curve fitting method. Based on the data from regression analysis, the energy transition temperature (ETT), which corresponds to the average value of upper shelf energy (USE) and lower shelf energy (LSE), was determined. In order to examine the cleavage fracture unit and crack propagation path, the fracture surface and the cross-sectional area beneath the fracture surface of the Charpy impact specimen fractured by cleavage at −196 °C were observed by a scanning electron microscope (SEM) after the fracture surface was coated by nickel.

The DWTT specimens had a size of 76.2 × 305 × 19.1 (full-plate-thickness) mm in the T-L direction in accordance with the API RP 5L3[11] specification, and then a pressed notch or a Chevron notch was machined into them. These specimens were tested using a DWTT testing machine with a maximum energy capacity of 20,000 J. The chamber was maintained at −15 °C by putting ethanol and spraying liquid nitrogen in it, where specimens were immersed for 20 minutes and then immediately tested. Figures 1(a) and (b) illustrate

Table I. Chemical Composition of the X70 Steel Used in this Study (Weight Percent)

C	Si	Mn	Cu + Ni + Mo	Nb + V + Ti	N
0.075	0.26	1.54	0.63	0.095 to 0.105	≤0.005

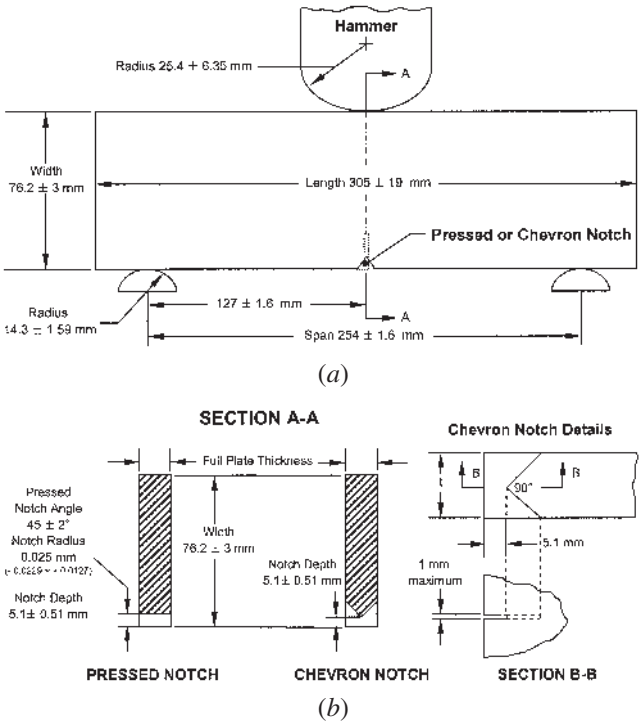

Fig. 1—Shape and dimensions of (*a*) the DWTT specimen and (*b*) its notch.

Table II. Rolling Conditions and Microstructures of the X70 Steel Specimens

Specimen	Finish Rolling Temperature (°C)	Start Cooling Temperature (°C)	Finish Cooling Temperature (°C)	Cooling Rate (°C/sec)	Microstructure*	Fraction of MA Constituent (Pct)	Fraction of RA (Pct)
A1	830 to 860	780 to 810	100	16.0	AF + QPF,BF	3.0	1.7
A2			200	19.0	AF + BF,QPF	3.3	2.5
A3			340	16.3	AF + BF,QPF	2.5	1.6
A4			430	9.4	AF + QPF	3.8	2.7
A5			480	14.1	AF + QPF	2.1	2.8
A6			580	12.4	AF + QPF	0.8	1.8
A7	720 to 750	690 to 710	100	12.5	PF + M	27.3	0.1
A8			240	14.5	PF + M,AF	22.5	0.6
A9			330	11.0	PF + AF,M	9.7	1.6
A10			420	9.3	PF + AF,BF	1.4	0.8
A11			505	12.0	PF + AF	0.9	0.1
A12			600	10.8	PF + WF	1.6	1.2

*Designation: major matrix + minor phases.

the shape and detailed dimensions of the DWTT specimen and its notch.

III. RESULTS

A. *Microstructure*

Microstructures in this study can be divided into polygonal ferrite (PF), quasi-polygonal ferrite (QPF), Widmanstätten ferrite (WF), acicular ferrite (AF), granular bainitic ferrite (GB), bainitic ferrite (BF), and martensite (M), in the order of decreasing transformation temperature.[17,18,19] The PF, transformed at the highest temperature, is an equiaxed microstructure, and QPF, transformed at a lower temperature than PF, has an irregular grain boundary. The WF is a plate-type microstructure initiated at and growing from austenite grain boundaries, while AF is an acicular microstructure formed inside austenite grains and has an irregular grain boundary. The GB contains equiaxed MA constituents, and has well-developed substructures inside. The BF has well-developed laths formed from austenite grain boundaries. Microstructures of the rolled specimens in this study were analyzed in terms of these categories.

Figures 2(a) through (f) are optical micrographs of the specimens rolled at the single-phase region (A1 to A6 specimens). Although the matrix of these specimens is composed of AF overall, the fraction of BF increases as the FCT goes below 430 °C (Figures 2(a) through (f)). In the A6 specimen fabricated at the highest FCT, the fraction of QPF having irregular grain boundaries increases (Figure 2(f)). Here, MA remains less than 1 pct, and the fraction of retained austenite (RA) is about 1.8 pct, while cementites is hardly observed. At the FCT lower than 430 °C, the fraction of MA increases to about 3 pct, but the fraction of RA stays at about 2 pct, irrespective of the FCT. The MA is sized by 0.5 to 3.0 μm, a little bit larger than RA sized by 0.5 to 1.0 μm. The MA is distributed mostly around prior austenite grain boundaries, and RA is observed at AF/AF or AF/QPF interfaces as well as prior austenite grain boundaries.

Figures 3(a) through (f) are optical micrographs of the specimens rolled at the two-phase region (A7 to A12 specimens). Unlike the specimens rolled at the single-phase region whose microstructure does not show much variation with the FCT change, PF, which was transformed prior to or during finish rolling, is present at about 68 pct in the specimens rolled at the two-phase region. Phases transformed from retained austenite during or after finish cooling, except PF, vary with FCT. In the A12 specimen fabricated at the FCT of 600 °C, WF is observed to be surrounded by PF transformed prior to cooling (Figure 3(f)). When the FCT goes down to about 400 °C, AF is primarily observed instead of WF (Figure 3(d)), and the fraction of martensite abruptly increases when the FCT goes down to temperatures lower than 330 °C (Figures 3(a) through (c)). Also, AF formed inside austenite grains during cooling is observed inside martensite. Black phases observed in the A12 specimen (Figure 3(f)) are cementites precipitated inside MA constituents. When hard phases such as MA or cementite are formed coarsely, stress is concentrated at them, and thus, low-temperature toughness can deteriorate.[20,21] With decreasing FCT, secondary phases tend to be reduced in their size and distributed homogeneously. In general, at the FCT higher than 420 °C, cementites are mostly observed at AF/AF interfaces or sub-boundaries (Figures 3(d) through (f)). At the FCT lower than 420 °C, cementites are rarely observed, but MA or RA phases are mostly found (Figures 3(a) through (c)). Basic microstructures, volume fractions of MA and RA of the specimens rolled at the single- and two-phase regions, are summarized in Table II.

Figure 4(a) is a transmission electron microscopy (TEM) bright-field image showing high-density dislocations formed near AF/MA interfaces of the A4 specimen. This is because lots of dislocations were formed inside nearby ductile AF as MA was transformed from RA by shear strain. They are mobile dislocations that can easily move and play a role in lowering yield strength since they induce materials to readily yield. Figure 4(b) is a TEM micrograph showing AF in the A11 specimen. Sub-boundaries composed of high-density dislocations and subunits composed of low-density dislocations are found inside AF grains. Figure 4(c) shows RA sized by about 1 μm in the A6 specimen, whose selected area diffraction pattern is presented in Figure 4(d).

B. *Tensile Properties*

Room-temperature tensile test results are provided in Table III and Figure 5. All the specimens show yield strength of above 483 MPa, regardless of rolling conditions, and satisfy the requirement of X70 grade pipeline steels. The yield ratio is below 0.85, which seems excellent overall. Tensile strength in all the specimens decreases in general as the FCT increases. Yield strength of the specimens rolled in the single-phase region increases with increasing FCT, reaches the maximum at 480 °C, and then decreases. In the specimens rolled in the two-phase region, yield strength is relatively high at the FCT of 240 °C and 420 °C, but it is about the same as in the specimens rolled in the single-phase region at other FCTs. Elongation tends to be disproportionate to yield strength, and is highest at the FCT of 580 °C for the specimens rolled in the single-phase region and 505 °C for the specimens rolled in the two-phase region.

C. *Charpy Toughness*

Figure 6 shows the absorption energy of Charpy impact test as a function of test temperature. Table IV lists the ETT and USE results obtained from Figure 6, and variation in impact absorption energy as a function of FCT is shown in Figure 7. Because of the inhomogeneity of steel specimens, scatters in the absorption energy *vs* test temperature are shown to be relatively large. Scatters in the specimens rolled in the single-phase region are slightly larger than those in the specimens rolled in the two-phase region. This may be because the inhomogeneity increases due to the longer cooling interval in the specimens rolled in the single-phase region than in the specimens rolled in the two-phase region.

The specimens rolled in the single-phase region show higher USE at all the FCT than the specimens rolled in the two-phase region. The ETTs of all the specimens are below −80 °C, and show excellent low-temperature toughness. The USE in the specimens rolled in the single-phase region gradually increases with increasing FCT, whereas the USE in the specimens rolled in the two-phase region reaches its

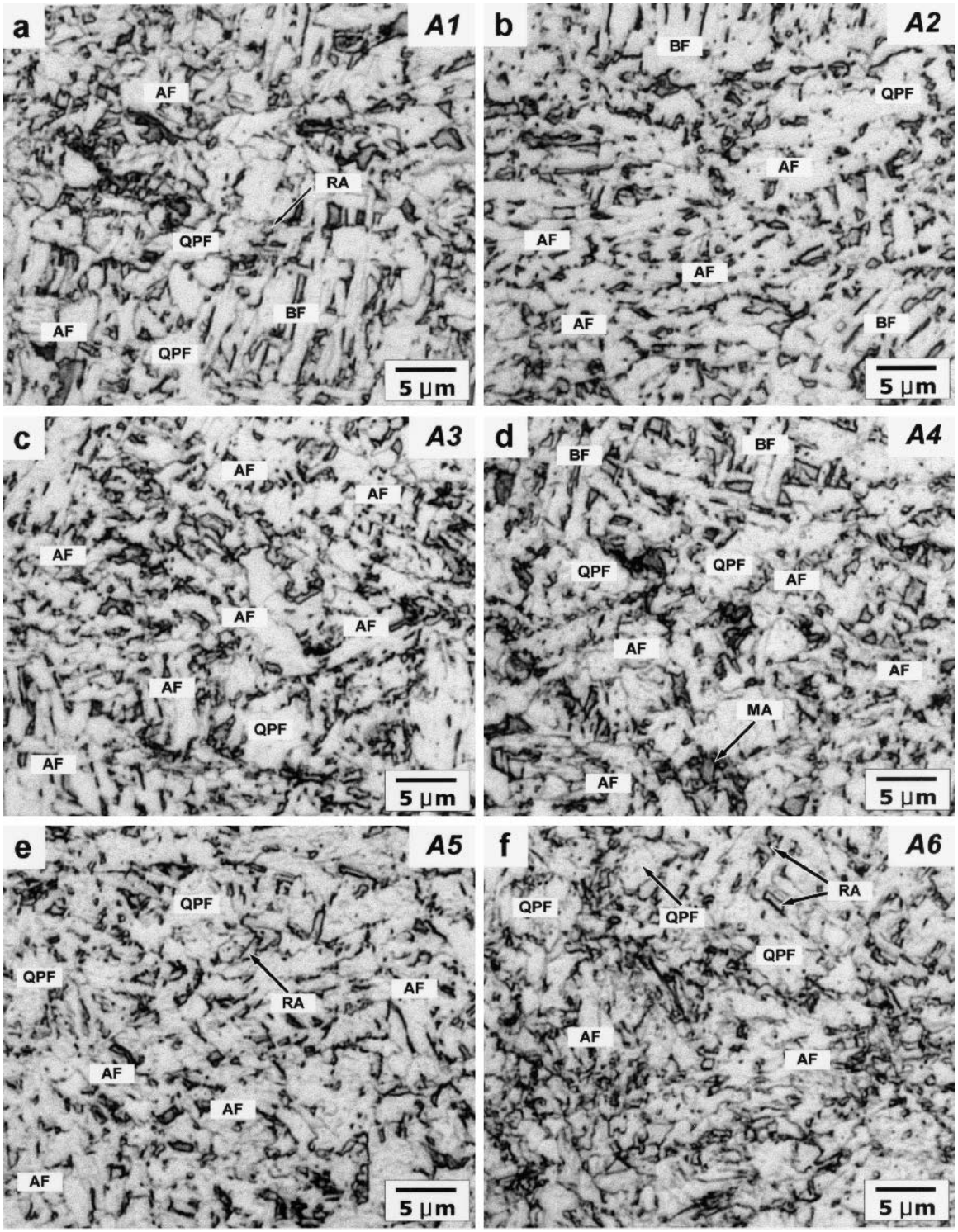

Fig. 2—Optical micrographs of the (*a*) A1, (*b*) A2, (*c*) A3, (*d*) A4, (*e*) A5, and (*f*) A6 specimens whose finish rolling temperature was 840 °C. Nital etched.

highest value at 420 °C and then decreases. All the specimens show excellent low-temperature toughness at the FCT of 300 °C to 500 °C. The ETT of the specimens rolled in the single-phase region is about the same (about −110 °C) at the FCT of 300 °C to 500 °C. In the specimens rolled in the two-phase region, the ETT at an FCT of 420 °C is the lowest (about −120 °C).

Variation in ETT can be confirmed from the results of cleavage fracture surfaces and cleavage crack propagation paths, as shown in Figures 8(a) through (f) and 9(a) through (f), respectively. The cleavage fracture unit of the A3 or A10 specimens showing the lowest ETT is about 10 μm, smaller than that of the A1 and A6 specimens or the A7 and A12 specimens, respectively (Figures 8(a) through (f)). The cleavage

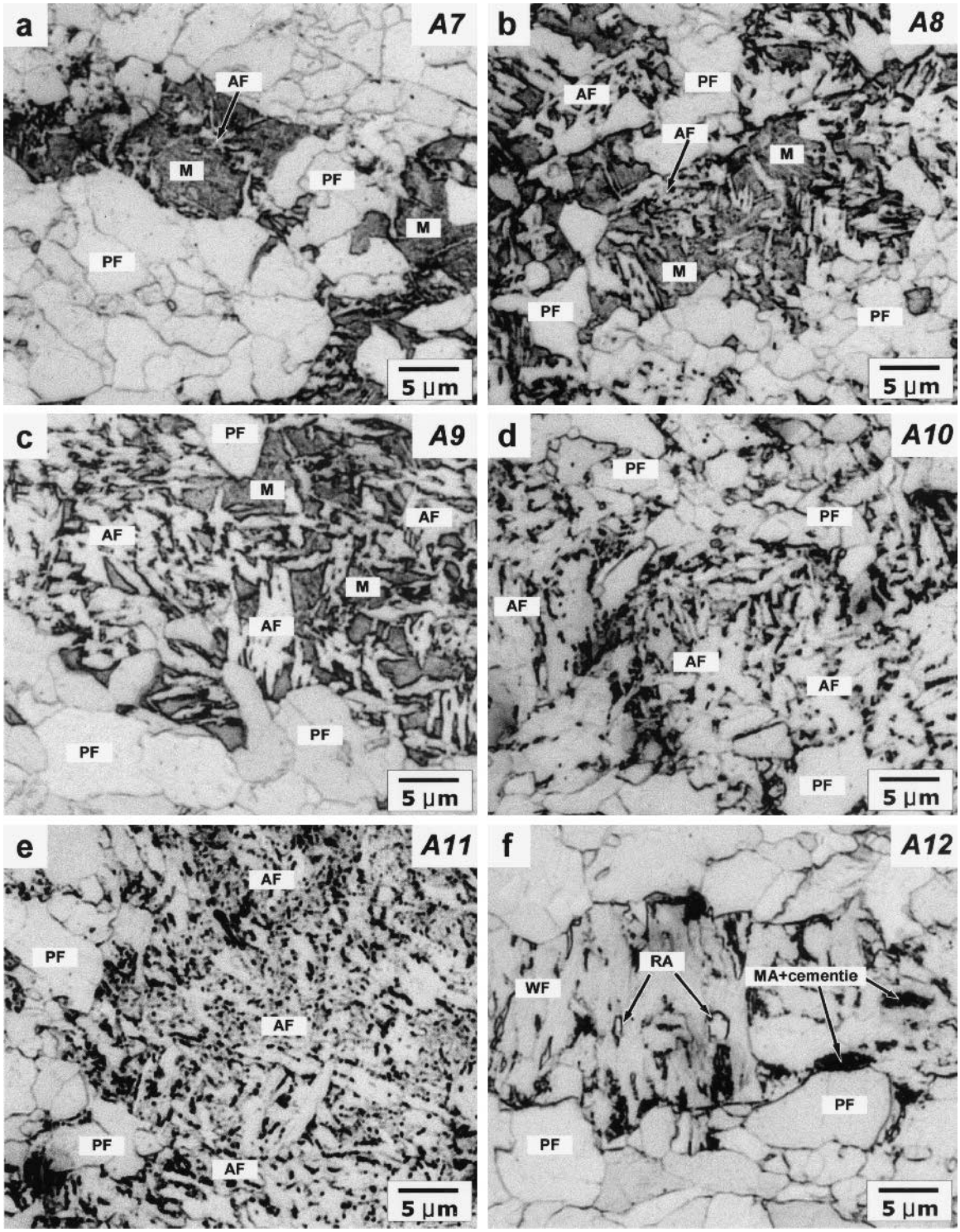

Fig. 3—Optical micrographs of the (*a*) A7, (*b*) A8, (*c*) A9, (*d*) A10, (*e*) A11, and (*f*) A12 specimens whose finish rolling temperature was 720 °C. Nital etched.

crack propagation path of the A4 and A10 specimens is more bent than that of other specimens (Figures 9(a) through (f)). This indicates that the A3 and A10 specimens have smaller effective grain size than others.

D. *DWTT Toughness*

Figures 10(a) through (d) show overall fracture surfaces of PN DWTT and CN DWTT specimens. The percent shear area (pct SA) was measured by an image analyzer from these fractographs, and the results are listed in Table IV. Variation in pct SA as a function of FCT is also shown in Figures 11(a) and (b). In the specimens rolled in the two-phase region, many separations take place on DWTT fractured surfaces (Figures 10(b) and (d)). Separations often occur in the steel plates fabricated by controlled rolling, and have some cleavage-type splits in the low-temperature ductile region because of

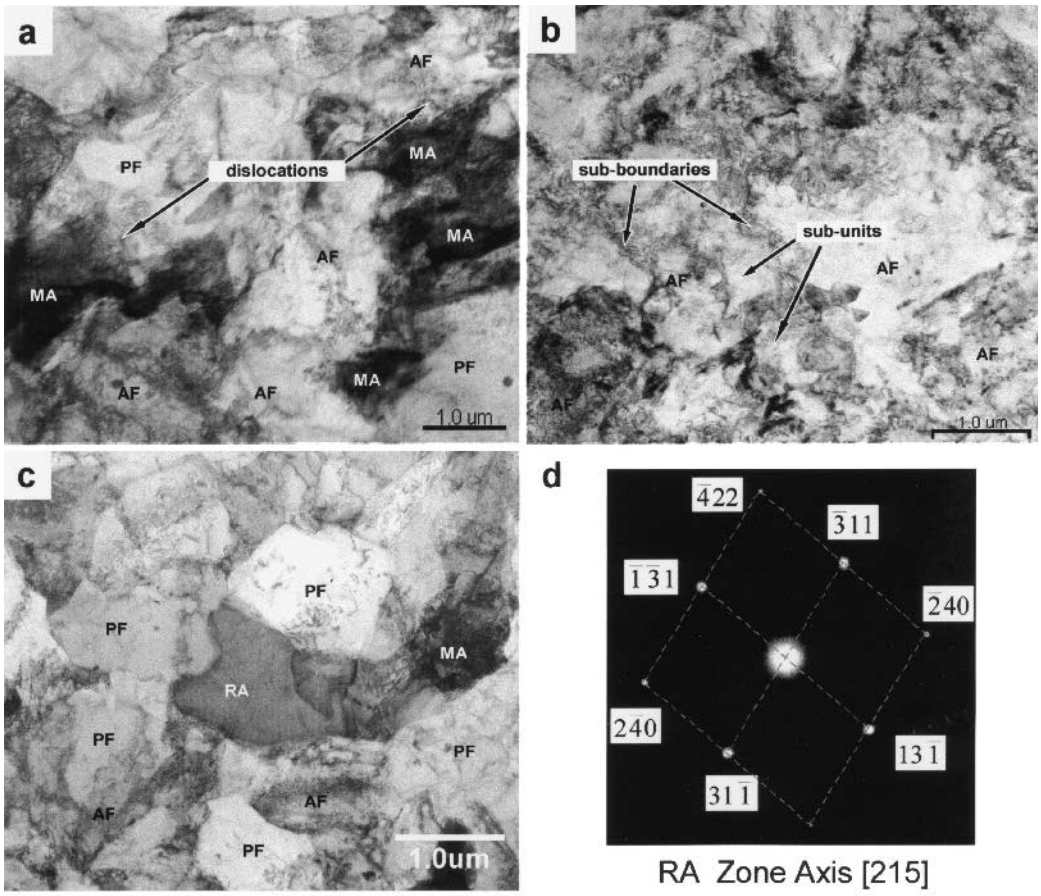

Fig. 4—TEM bright-field images showing (*a*) high-density dislocations formed at AF/MA interfaces in the A4 specimen, (*b*) AF composed of sub-boundaries and subunits in the A11 specimen, and (*c*) RA in the A6 specimen. (*d*) SADP of RA in (c). The pattern was obtained from RA [215] zone axis.

Table III. Room-Temperature Tensile Properties of the X70 Steel Specimens

Specimen	Yield Strength (MPa)	Tensile Strength (MPa)	Elongation (Pct)	Yield Ratio
A1	516	756	28.9	0.68
A2	523	744	25.7	0.70
A3	531	746	24.2	0.71
A4	525	730	25.6	0.72
A5	566	691	24.4	0.82
A6	539	703	30.1	0.77
A7	508	754	25.9	0.67
A8	533	776	24.8	0.69
A9	489	715	27.1	0.68
A10	561	697	25.0	0.81
A11	517	663	27.6	0.78
A12	491	664	26.1	0.74

the high triaxial stress state in the necked plastic region.[22] In the case of the specimens rolled in the two-phase region, a band structure easily forms as some polygonal ferrite grains formed at austenite grain boundaries were elongated during rolling, thereby leading to the frequent formation of separations on fracture surfaces. In the hammer-impacted region of most DWTT specimens, inverse fracture of cleavage type is found (Figures 10(a) through (d)). This inverse fracture is a fracture mode having a cleavage fracture area in the region

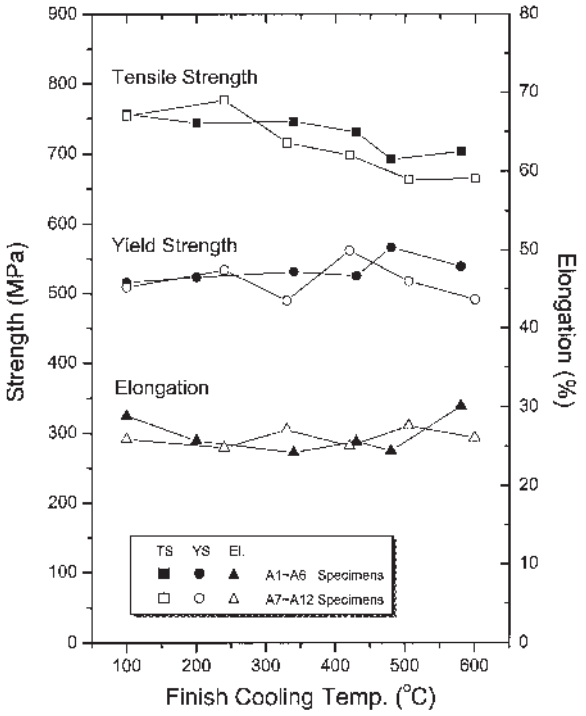

Fig. 5—Tensile strength, yield strength, and elongation *vs* finish cooling temperature.

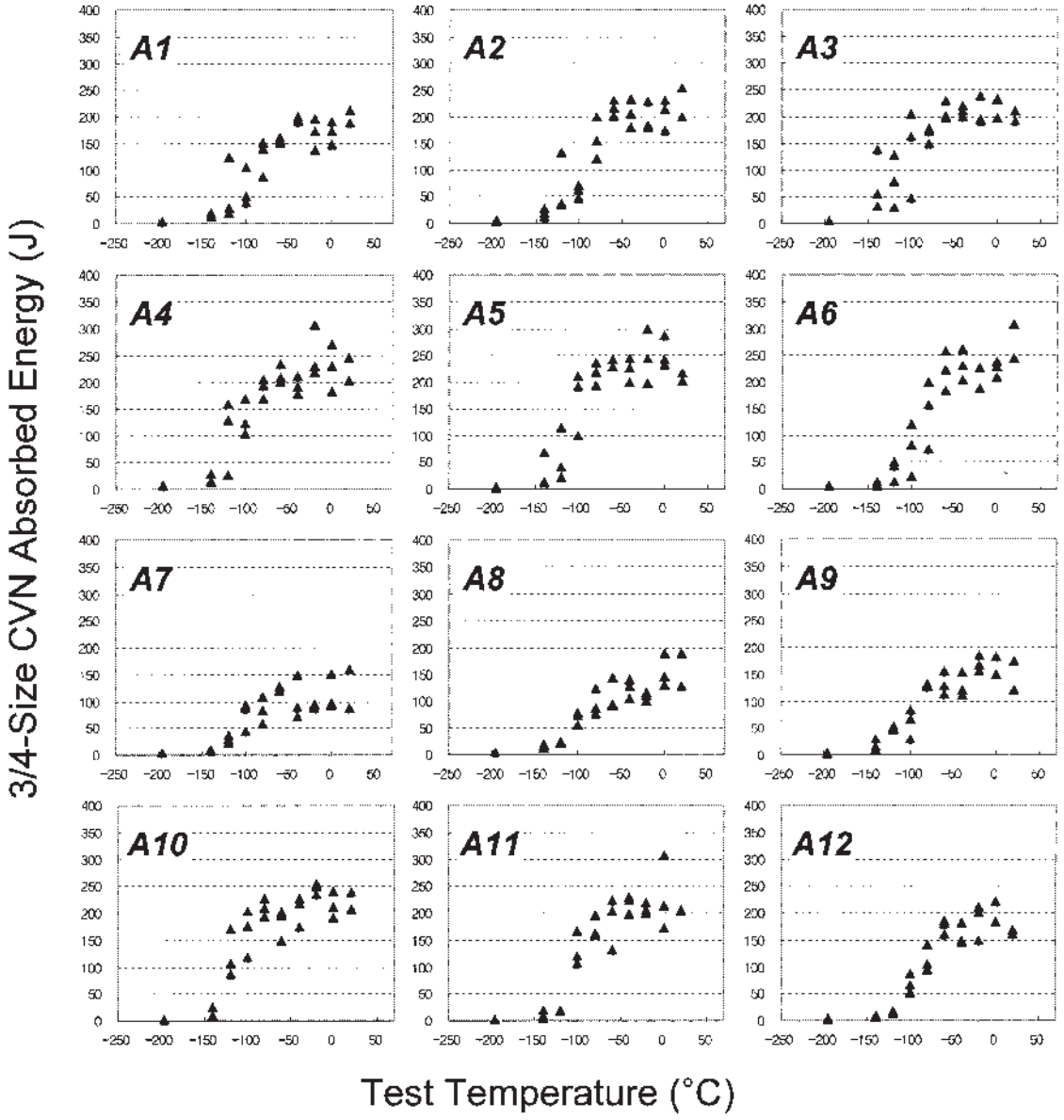

Fig. 6—Charpy V-notch impact energy *vs* test temperature.

Table IV. Fracture Properties of the X70 Steel Specimens

	CVN Properties		DWTT Pct Shear Area*	
Specimen	USE (J)	ETT (°C)	PN DWTT	CN DWTT
A1	185.3	−92.2	98.0	99.6
A2	210.2	−88.1	98.9	100.0
A3	217.6	−111.9	97.6	99.2
A4	228.9	−110.3	98.5	99.9
A5	235.6	−107.9	92.7	98.5
A6	238.5	−87.2	79.1	92.7
A7	109.8	−107.1	96.5	98.5
A8	148.2	−92.6	97.8	95.0
A9	156.3	−97.7	99.2	95.4
A10	214.4	−120.8	95.4	89.5
A11	210.2	−102.5	97.9	91.4
A12	182.7	−90.0	95.0	96.2

*Percent shear area under API 5L3 specification.

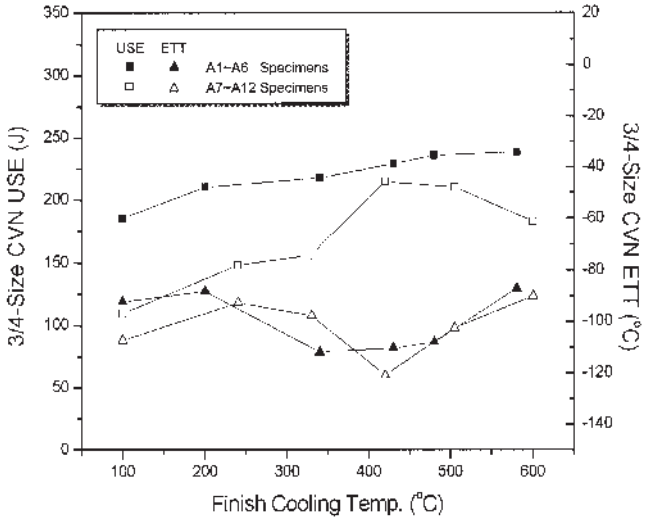

Fig. 7—USE and ETT *vs* finish cooling temperature.

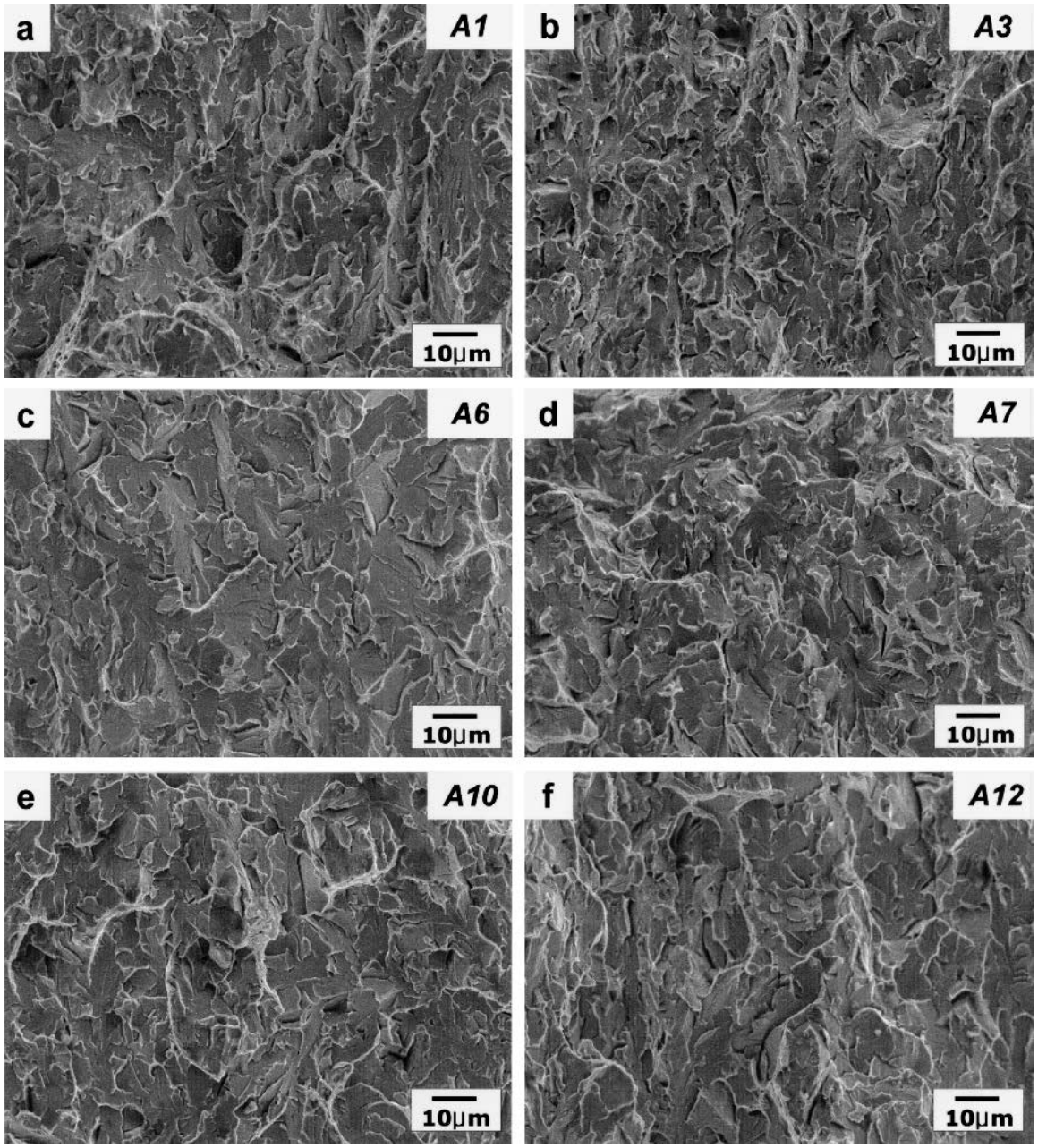

Fig. 8—SEM fractographs of Charpy impact specimens fractured at −196 °C for the (*a*) A1, (*b*) A3, (*c*) A6, (*d*) A7, (*e*) A10, and (*f*) A12 specimens.

impacted by a hammer after the initiation of cleavage fracture at the notch, and is generally known to be formed mainly by work hardening due to hammer impact.[7] All the specimens were valid in accordance with the API 5L3 specification since cleavage fracture was initiated from the notch, irrespective of the kind of DWTT, and the pct SA was calculated including the inverse fracture. The cleavage fracture surfaces formed at the notch in the CN DWTT were somewhat larger than those in PN DWTT because of higher stress concentration at the Chevron notch.[23]

The pct SA of all the specimens except the A6 specimen is over 85 pct, regardless of the kind of notch, and shows excellent DWTT properties (Table IV). The pct SA of the PN DWTT in the specimens rolled in the single-phase region is lower than that of the CN DWTT at all the FCT. The pct SA of both DWTT stays almost constant up to the FCT of 400 °C, and tends to abruptly drop at the FCT higher than 500 °C (Figure 11(a)). In the specimens rolled in the two-phase region, the variation in the pct SA of both DWTT is similar, and the pct SA is the lowest at an FCT of 420 °C.

IV. DISCUSSION

Though there are some variations in the 12 X70 steel specimens fabricated in this study, depending on rolling conditions, they all show excellent low-temperature toughness, high absorption energy, low DBTT, and high DWTT pct SA. In

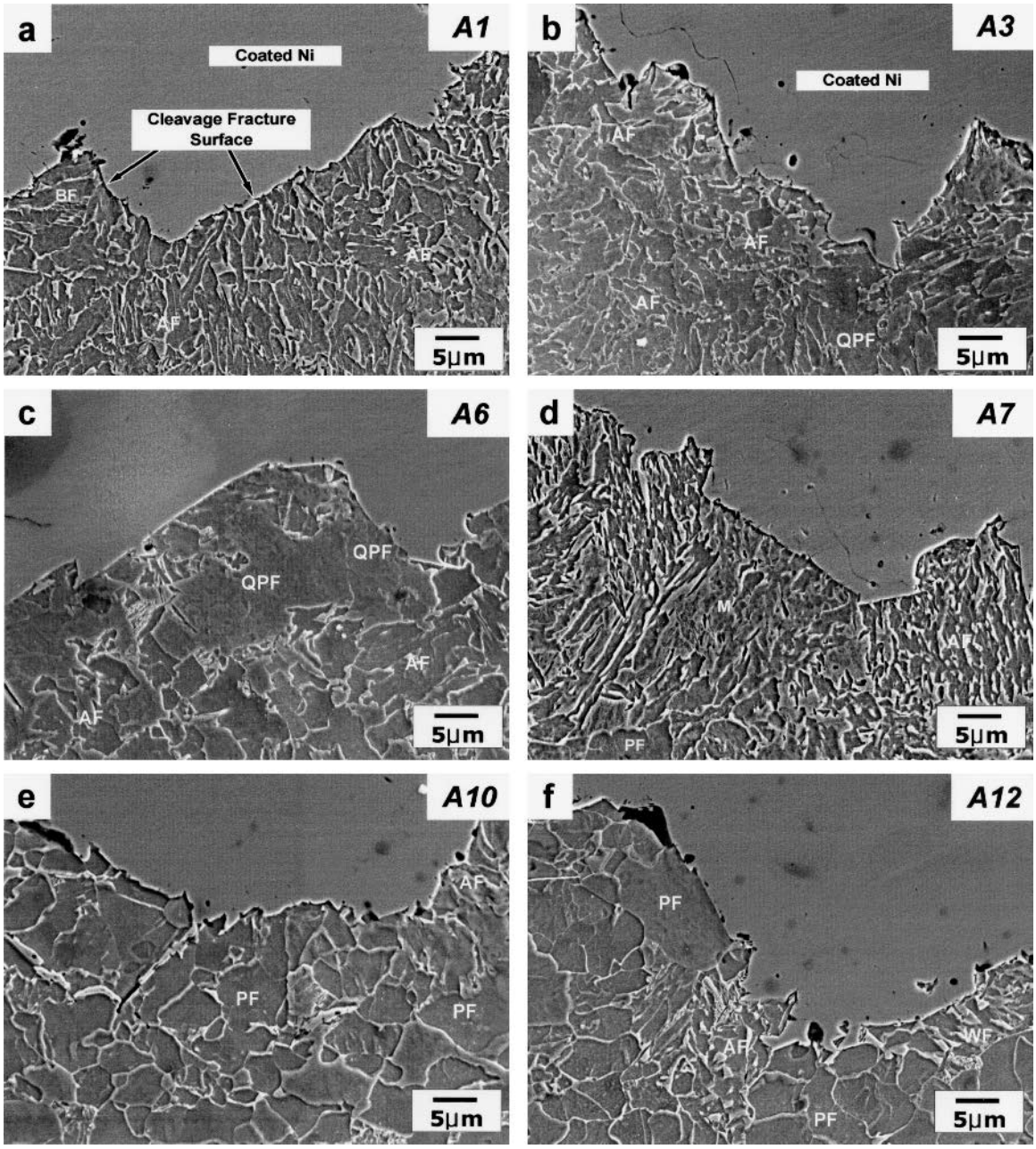

Fig. 9—SEM micrographs of the cross-sectional area beneath the cleavage fracture surface of Charpy impact specimens fractured at −196 °C for the (*a*) A1, (*b*) A3, (*c*) A6, (*d*) A7, (*e*) A10, and (*f*) A12 specimens, showing the crack propagation path. Fractured surfaces were coated by Ni.

this study, microstructural factors such as kind, volume fraction, and size of phases and effective grain size are analyzed to study how they affect the absorption energy, DBTT, and DWTT properties.

The USE of all the specimens rolled in the single-phase region (A1 to A6 specimens) is higher than that of the specimens rolled in the two-phase region (A7 to A12 specimens) at all the FCT. This is because many dislocations are produced inside PF in the specimens rolled in the two-phase region when a large amount of PF transformed prior to finish rolling was deformed during finish rolling, and thus, the absorption energy of PF is lower than that of AF formed in the specimens rolled in the single-phase region. Since the matrix of the specimens rolled in the single-phase region mainly consists of AF, they have higher absorption energy, and hardly show variations in microstructures and USE with varying FCT. However, since the volume fraction of BF having low absorption energy increases with decreasing FCT, the USE gradually decreases, and is the highest at the FCT of 600 °C because of the formation of a small amount of high-toughness QPF.

The USE in the specimens rolled in the two-phase region is greatly affected by other phases as well as by PF formed prior to cooling. At the lower FCT between 100 °C and 300 °C, brittle martensite is formed from austenite present after finish rolling, thereby showing the low absorption

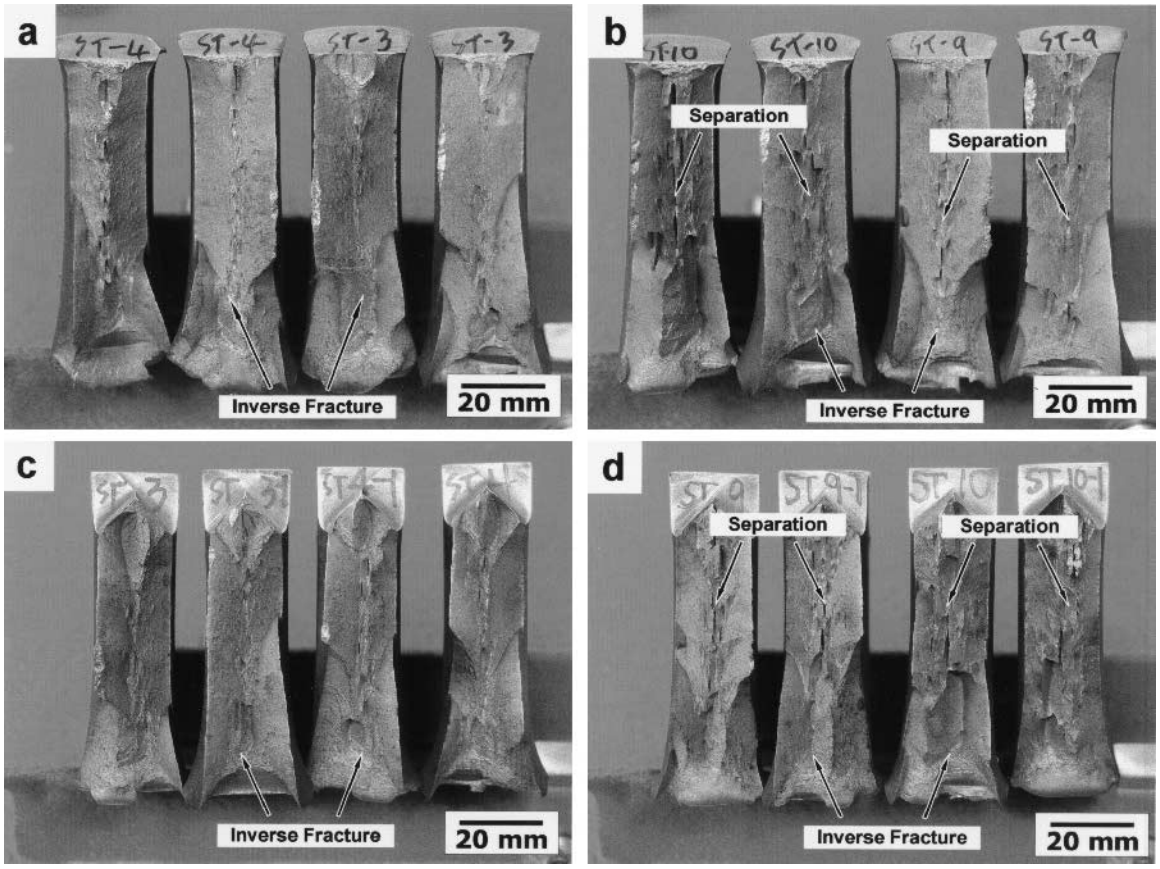

Fig. 10—Overall fracture surfaces appeared in (*a*) and (*b*) PN DWTT specimens and (*c*) and (*d*) CN DWTT specimens.

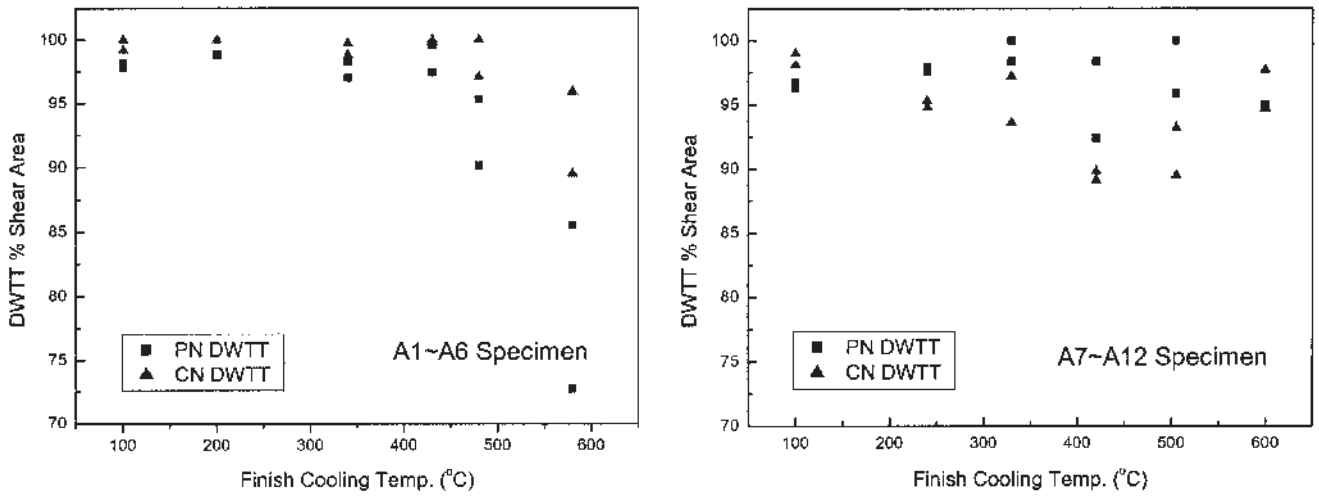

Fig. 11—Percent shear area of the fractured DWTT specimens of the (*a*) A1 to A6 specimens and (*b*) A7 to A12 specimens *vs* finish cooling temperature.

energy. At the FCT of 600 °C, cementite and MA are coarsely formed together with WF, which negatively affects the absorption energy.[20,21] Thus, the USE in the specimens rolled in the two-phase region reaches the maximum at the FCT of 400 °C 500 °C because much high-toughness AF are formed as in the specimens rolled in the single-phase region.

In general, the absorption energy of the Charpy impact test is affected by microstructural factors such as kind, volume fraction, and size of secondary phases and matrix, and the effective grain size is a main microstructural factor affecting DBTT such as ETT.[22–29] Therefore, this study intended to interpret the variation in ETT in terms of effective grain size. Since all the specimens in this study were fabricated with

the rolling reduction ratio of 75 pct in the nonrecrystallization region of austenite to achieve the grain refinement effect, they are expected to show excellent low-temperature toughness. Indeed, the ETT of all the specimens is below −80 °C, and reaches as low as −110 °C to 120 °C at the FCT of 300 °C to 500 °C, showing excellent low-temperature toughness.

The ETT variations *vs* FCT are described as follows. In the specimens rolled in the single-phase region, the ETT does not vary much because the matrix is mostly composed of AF, but shows a slight change due to some phases formed by the FCT change. In the low FCT of 100 °C to 200 °C, the volume fraction of BF, which is a low-temperature transformed microstructure, increases and cleavage fracture proceeds ahead without changing its path at BF lath boundaries, thereby resulting in larger effective grain size (Figure 9(a)). Subunits inside AF grains have the same orientation, but those between the nearest AF grains have different orientations. Thus, AF has excellent low-temperature toughness as its grain size decreases. This can be exactly confirmed in the EBSD analysis data on the A5 specimen of Figure 12(a). Observation of grains having misorientation larger than 15 deg as demarked by black lines in Figure 12(a) reveals that effective grain size is somewhat large when there are many subunits inside AF grains. Most AF grains have very small effective grain size as they have different orientation from nearby AF. At the FCT higher than 600 °C, the grain size of AF slightly increases, coarse QPF are formed, and thus the ETT and effective grain size increase (Figure 9(c)). Consequently, out of the specimens rolled in the single-phase region, the A3 to A5 specimens have the lowest ETT and small cleavage fracture unit (about 10 μm) because of the formation of a large amount of AF having small effective grain size (Figures 7 and 8(b)).

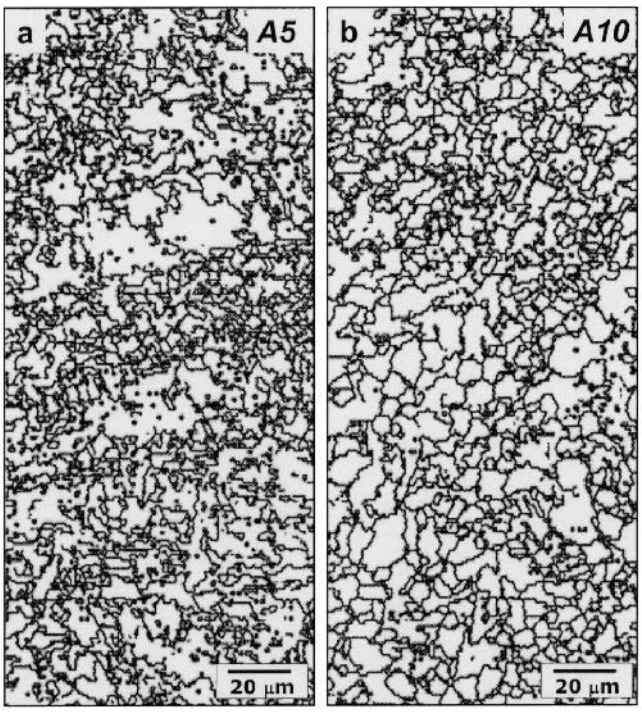

Fig. 12—EBSD analysis data of the (*a*) A5 and (*b*) A10 specimens, showing grains having misorientation larger than 15 deg.

In the specimens rolled in the two-phase region, overall effective grain size is largely determined by PF (about 68 vol pct) formed before or during finish rolling, as mentioned earlier, irrespective of FCT. Thus, the ETT does not vary much with FCT, as in the specimens rolled in the single-phase region. At the low FCT of 100 °C to 300 °C, martensite transformed from retained austenite is formed, and its effective grain size is in general about the same as prior austenite grain size. Therefore, the effective grain size of the A7 to A9 specimens, where martensite was formed overall, increases, consequently leading to higher ETT. Since relatively coarse WF and PF are formed at the high FCT of 600 °C, the ETT also increases. The ETT at the FCT of 420 °C is extremely low at −120 °C. This is because overall effective grain size considerably decreases since 10-μm-sized fine PF coexists with AF having small effective grain size. Examination of the crack propagation path of the A10 specimen in Figure 9(e) reveals that PF is found to be effective to turn the crack propagation path. It is because PF has misorientations of high-angle boundary as seen in the EBSD analysis data of Figure 12(b).

According to the DWTT results, the pct SA of PN DWTT and CN DWTT shows a similar tendency with varying FCT, and all the specimens except the A6 specimen show 85 pct or higher shear area (Figures 11(a) and (b)). This is because most cleavage fracture is not included in the calculation of the pct SA as cleavage cracks are mostly arrested within 19.1 mm after cleavage fracture was initiated at the notch of DWTT specimens.[11] Since inverse fracture occurred in the hammer-impacted region of most of the DWTT specimens and it was included in the calculation of pct SA in accordance with the API 5L3 specification, the pct SA is mostly below 100 pct. Consequently, the pct SA of the steel specimens having inverse fracture is greatly affected by the inverse fracture formation.

The SA pct of DWTT varies with the kind of DWTT. CN DWTT specimens show relatively higher pct SA in the specimens rolled in the single phase-region, whereas PN DWTT specimens show higher pct SA in the specimens rolled in the two-phase region. Though it is recommended to use PN DWTT specimens for low-toughness steels, while using CN DWTT specimens for high-toughness steels, according to the current API 5L3 specification, there are no clear guidelines on the use of these different DWTT specimens. Thus, the difference in SA pct arising from different DWTT specimens can cause critical problems on the matter of guaranteeing low-temperature toughness of pipeline steels between suppliers and users. Further studies are required to establish new standards on the selection of DWTT according to material properties.

Inverse fracture is heavily formed at the FCT of 580 °C and 420 °C for the specimens rolled in the single-phase region and the specimens rolled in the two-phase region, respectively, at which the absorption energy is the highest and the pct SA is the lowest. This indicates that the formation of inverse fracture is indirectly related to the toughness of steels. This can be guessed from the fact that inverse fracture occurs largely in high-toughness pipeline steels recently under development. These inverse fractures occurring during DWTT are often observed in many pipeline steels recently developed, and are serious as pipeline steels become tougher, thicker, and larger.[7,30–33] In the case of

serious inverse fracture, as observed in the specimens of this study, it can adversely affect DWTT properties, and thus, the issue of inclusion or exclusion of inverse fracture needs immediate attention. Since the current API 5L3 specification does not mention the inverse fracture, it engenders much controversy among researchers. However, because many researchers are in agreement when claiming the work-hardening effect due to the impact of hammer as the primary cause for the formation of inverse fracture, it is feasible to revise the evaluation methods of DWTT. Since prestrain due to work hardening inside the specimen does not exist in the practical conditions of pipeline steels, it seems desirable to exclude inverse fracture occurring during DWTT from the calculation of pct SA. The steel specimens of this study show excellent DWTT properties with pct SA close to 100 pct, when inverse fracture is not included in calculating pct SA.

The experimental results indicate that microstructures, which appropriately contain AF having high absorption energy together with fine PF having high-angle grain boundary, show excellent low-temperature toughness. However, when inverse fracture occurs in the hammer-impacted region due to a too high absorption energy during DWTT, DWTT properties can rather deteriorate. All the specimens in this study pose problems in evaluating DWTT properties due to the occurrence of inverse fracture. It seems that these problems will become more serious in the future as DWTT temperature decreases and pipeline steels become tougher, thicker, and larger. Therefore, efforts are required in the future to modify the presently used DWTT or to develop new testing methods[34,35,36] so as to more accurately predict the actual FPTT of pipeline steels and to properly evaluate the resistance to unstable ductile fracture propagation.

V. CONCLUSIONS

The X70 grade steel specimens having different microstructures were fabricated by varying rolling conditions, and correlation of their microstructures with tensile, Charpy impact, and DWTT properties was investigated.

1. The Charpy impact test results showed that the USE of the specimens rolled in the two-phase region was lower than that of the specimens rolled in the single-phase region because a large amount of PF was formed prior to cooling. As the microstructure of the specimens rolled in the single-phase region did not change much with varying FCT, the USE did not change much. On the other hand, in the specimens rolled in the two-phase region, it changed much as martensite, AF, and WF as well as PF were formed here.
2. The ETT obtained from the Charpy impact test of all the specimens was below −100 °C at the FCT of 350 °C to 500 °C, and showed excellent low-temperature toughness. However, the ETT increased because of the increased effective grain size due to the formation of low-temperature transformation phases such as BF and martensites at the lower FCT and because of the formation of coarse ferrites such as WF and QPF at the higher FCT.
3. The ETT at the FCT of 420 °C was extremely low (about −120 °C) in the specimens rolled in the two-phase region. This was because fine PF having high-angle grain boundary was formed due to high rolling reduction ratio in the nonrecrystallization region, and because the overall effective grain size decreased due to the presence of AF having smaller effective grain size.
4. The pct SA of DWTT of all the specimens was mostly over 85 pct, and showed excellent DWTT fracture properties. Irrespective of finish rolling temperature, the pct SA of PN DWTT and CN DWTT specimens showed a similar trend with varying FCT. The specimens rolled in the single-phase region showed the lowest pct SA at the FCT of 580 °C where the absorption energy was the highest, while the specimens rolled in the two-phase region showed the lowest pct SA at the FCT of 420 °C, as a large amount of inverse fracture occurred at these FCTs.

ACKNOWLEDGMENTS

This work was financially supported by the National Research Laboratory Program of the Ministry of Science and Technology of Korea and by POSCO under Contract No. PL-03909. The authors thank Drs. Wung Yong Choo, Chong Soo Woo, Dong Han Suh, and Sung Soo Ahn, POSCO, and Professor Kwang Sun Shin, Seoul National University, for their help of the testing and data analyses of DWTT.

REFERENCES

1. R. Denys: *Pipeline Technology*, Elsevier, Brugge, Belgium, 2000, vols. I–II.
2. J.E. Hood: *Int. J. Pres. Ves. Piping*, 1974, vol. 2, pp. 165-78.
3. J.Y. Koo, M.J. Luton, N.V. Bangaru, R.A. Petkovic, D.P. Fairchild, C.W. Petersen, H. Asahi, T. Hara, Y. Terada, M. Sugiyama, H. Tamehiro, Y. Komizo, S. Okaguchi, M. Hamada, A. Yamamoto, and I. Takeuchi: *ISOPE Symp. High-Performance Materials in Offshore Industry*, Honolulu, HI, 2003, pp. 10-18.
4. M. Matsuda and H. Miura: *Met. Mater. Int*., 2003, vol. 9, pp. 537-42.
5. K.T. Corbett, R.R. Bowen, and C.W. Petersen: *ISOPE Symp. High-Performance Materials in Offshore Industry*, Honolulu, HI, 2003, pp. 105-12.
6. H.N. Han, C.-S. Oh, D.W. Suh, C.G. Lee, T.-H. Lee, and S.-J. Kim: *Met. Mater. Int*., 2004, vol. 10, pp. 221-29.
7. G. Mannucci, and D. Harris: "*Fracture Properties of API X100 Gas Pipeline Steels*", Final Report, European Commission, Brussels, Belgium, 2002, pp. 1-128.
8. G.M. McClure, A.R. Duffy, and R.J. Eiber: *J. Eng. Industry*, 1965, vol. 4, pp. 265-78.
9. G.M. Wilkowski, W.A. Maxey, and R.J. Eiber: *ASM Symp. on What Does Charpy Test Really Tell Us*?, ASM, Metals Park, OH, 1978, pp. 201-25.
10. G.M. Wilkowski, W.A. Maxey, and R.J. Eiber: *Can. Metall. Q*., 1980, vol. 19, pp. 59-77.
11. *API Recommended Practice 5L3*, American Petroleum Institute, Washington, DC, 1996.
12. D.J. Horsley: *Eng. Fract. Mech*., 2003, vol. 70, pp. 547-52.
13. R.J. Eiber, T.A. Bubenik, and W.A. Maxey: *Fracture Control Technology For Natural Gas Pipelines*, Pipeline Research Council International Inc., Arlington, VA, 1993.
14. *ASTM Standard E23-02*, ASTM, West Conshohocken, PA, 2002.
15. T.-H. Lee, C.-S. Oh, C.G. Lee, S.-J. Kim, and S. Takaki: *Met. Mater. Int*., 2004, vol. 10, pp. 231-36.
16. A.K. De, J.G. Speer, and D.K. Matlock: *Adv. Mater. Process*, 2003, vol. 161, pp. 27-30.
17. *Atlas for Bainitic Microstructures*, Iron Steel Inst. Jpn., Tokyo, 1992, vol. 1.
18. T. Hayashi, F. Kawabata, and K. Amano: *Proc. Materials Solution '97 on Accelerated Cooling/Direct Quenching of Steels*, ASM INTERNATIONAL, Materials Park, OH, 1997, pp. 93-99.

19. G. Krauss and S.W. Thompson: *Iron Steel Inst. Jpn. Int*., 1995, vol. 35, pp. 937-45.
20. B.C. Kim, S. Lee, N.J. Kim, and D.Y. Lee: *Metall. Trans. A*, 1991, vol. 22A, pp. 139-49.
21. S. Kim, S. Lee, Y.-R. Im, H.-C. Lee, S.-J. Kim, and J.H. Hong: *Metall. Mater. Trans. A*, 2004, vol. 35A, pp. 2027-37.
22. I. Tamura, H. Sekine, T. Tanaka, and C. Ouchi: *Thermomechanical Processing of High-strength Low-Alloy Steels*, Butterworth & Co. Ltd., London, 1988.
23. G.E. Dieter: *Mechanical Metallurgy*, McGraw-Hill, London, 1988.
24. J.M. Hyzak and I.M. Bernstein: *Metall. Trans. A*, 1976, vol. 7A, pp. 1217-24.
25. N.J. Kim: *J. Met*., 1983, vol. 35, pp. 21-27.
26. N.J. Kim, A.J. Yang, and G. Thomas: *Metall. Trans. A*, 1985, vol. 16A, pp. 471-74.
27. Y.M. Kim, S.K. Kim, Y.J. Lim, and N.J. Kim: *Iron Steel Inst. Jpn. Int*., 2002, vol. 42, pp. 1571-77.
28. C.-S. Oh, H.N. Han, C.G. Lee, T.-H. Lee, and S.-J. Kim: *Met. Mater. Int*., 2004, vol. 10, pp. 399-406.
29. B. Hwang, S. Lee, Y.M. Kim, N.J. Kim, and S.S. Ahn: *Metall. Mater. Trans. A*, 2005, vol. 36A, pp. 725-39.
30. N. Iwasaki, T. Yamaguchi, and T. Taira: *Mech. Work Steel Process*, 1975, vol. 13, pp. 294-314.
31. H. Kashimura, M. Ogasawara, and H. Mimura: *Met. Progr*., 1976, Nov., pp. 58-62.
32. K. Seifert: *Mater. Testing*, 1984, vol. 26, pp. 277-80.
33. B. Hwang, S. Lee, Y.M. Kim, N.J. Kim, J.Y. Yoo, and C.S. Woo: *Mater. Sci. Eng. A*, 2004, vol. A368, pp. 18-27.
34. F. Rivalin, A. Pineau, M.D. Fant, and J. Besson: *Eng. Fract. Mech*., 2001, vol. 68, pp. 329-45.
35. P. Salvini, A. Fonze, and G. Mannucci: *Eng. Fract. Mech*., 2003, vol. 70, pp. 553-66.
36. M. Toyoda and R. Denys: *Proc. Int. Pipe Dreamer's Conf*., Scientific Surveys, Ltd., Yokohama, Japan, 2002.